

ICANS-XVI

16th Meeting of the International Collaboration on Advanced Neutron Sources

May 12 – 15, 2003

Düsseldorf-Neuss, Germany

The QuasiElastic Neutron Spectrometer (QENS) of IPNS: Recent Upgrade and Performance

R. W. Connatser Jr.¹, H. Belch¹, L. Jirik¹, D. J. Leach¹, F. R. Trouw^{1,*}, J.-M. Zanotti^{1,§}, Y. Ren^{1,†}, R. K. Crawford¹, J. M. Carpenter¹, D. L. Price^{1,¶}, C.-K. Loong¹, J. P. Hodges^{2,3}, and K. W. Herwig²

¹*Intense Pulsed Neutron Source Division, Argonne National Laboratory, Argonne, IL 60439 USA*

²*Spallation Neutron Source Project and ³Metals and Ceramics Division, Oak Ridge National Laboratory, Oak Ridge, TN 37831 USA*

Abstract

The upgrade of the QuasiElastic Neutron Spectrometer (QENS) at the Intense Pulsed Neutron Source (IPNS), which replaced the 3 detector arms in a previous configuration with 22 crystal-analyzer-detector arrays outfitted with cooled beryllium-filters in a new scattering chamber, was completed. An average energy resolution (FWHM) varying from 80 μeV (elastic) to 4-5% of the energy transfer (inelastic, up to ~ 200 meV neutron energy loss) is maintained over a wide range of wavevectors from 0.3 to 2.5 \AA^{-1} . The diffraction patterns (total scattering) from 0.1 to 30 \AA^{-1} are measured concurrently by two additional detector clusters. We report the design, operation, and data-analysis software of this upgraded spectrometer. We describe the performance capabilities of QENS based on our experience in serving users since mid-2001. The installation of a funnel guide for the incident beam currently under way and future enhancements will be discussed.

1. Introduction

The QuasiElastic Neutron Spectrometer (QENS) at the Intense Pulsed Neutron Source (IPNS) of Argonne National Laboratory, a crystal-analyzer spectrometer originally designed, constructed and commissioned in 1986, was to favor high neutron flux at the sample and to view large scattering solid angles via a mosaic of analyzer crystals by the detectors.[1] By virtue of the time-of-flight technique, these parameters were chosen to satisfy as close as possible the "time-focusing conditions" under which the sample-to-detector flight time is constant, hence minimize the time uncertainty contributions to the energy resolution. However, the layout of the QENS permitted only three detector arms, housing a total of 35 cylindrical ^3He detectors. Only a small portion of the scattering angles is covered at each setting. Collection of data over the full Q-range would require several measurements each conducted at a different scattering angle setting by rotating the entire detector-arm unit. Furthermore, the sample-analyzer-detector distances in the third arm are shorter than those in

* Present and permanent address: The Lujan Center, Los Alamos National Laboratory, Los Alamos, NM 87545 USA.

§ Permanent address: Laboratoire Léon Brillouin (CEA-CNRS), CEA Saclay, 91191 Gif/Yvette cedex, France

† Present address: Materials Science Division, Argonne National Laboratory, Argonne, IL 60439 USA.

¶ Present address: CNRS UPR 4212, 45071 Orleans Cedex 2, France.

the other two, resulting in a somewhat lower resolution. Although QENS operated as an IPNS user instrument for over a decade and was improved incrementally over the years, these limitations hindered the effectiveness of $S(Q, E)$ measurements. Meanwhile, the demand in the US for quasielastic neutron-scattering studies of chemical and biological systems has increased steadily. This motivated us to upgrade the spectrometer with a new design of analyzer-detector assembly, aiming for highly efficient measurements of $S(Q, E)$ over a wide (Q, E) range with good, uniform energy resolution.

2. Design features, layout and resolution

The design features of the upgraded QENS include 22 crystal-analyzer-detector arms outfitted with cooled beryllium-filters in a new scattering chamber, yielding a uniform energy resolution (FWHM) varying from $\sim 80 \mu\text{eV}$ (elastic) to 4-5% of the energy transfer (inelastic, up to $\sim 200 \text{ meV}$ neutron energy loss) over a wide range of wavevectors from 0.3 to 2.5 \AA^{-1} . Two additional detector clusters measure concurrently the diffraction patterns (total scattering) over the $0.1 < Q < 30 \text{ \AA}^{-1}$ region. A total of 146 ^3He cylindrical detectors are employed. The new QENS has been fully operational since mid-2001 as a user instrument. Its performance capability, such as data-collection time, ease of operation, and data-analysis, has been enhanced by a factor of 3 to 5 in comparison with the previous configuration.

Fig. 1 shows a schematic layout of QENS. At the entrance, the evacuated beam tube views the entire surface ($\sim 100 \text{ mm}$ wide and $\sim 100 \text{ mm}$ high) of the IPNS H-moderator (solid methane at $\sim 20 \text{ K}$) at 90° . Downstream over an incident flightpath (ℓ_1) of 8.05 m the beam area is tapered to a width of 12.7 mm and a height of 101.6 mm in front of the sample position. The analyzer arrays, beryllium-filter tanks, detectors and preamplifier electronics are housed inside a shielded scattering chamber that is under a flowing-nitrogen atmosphere at ambient pressure. The sample environment, normally under high vacuum, is separated from the scattering chamber by thin ($\sim 1 \text{ mm}$ thick) aluminum windows. The entrance and exit windows for the direct beam are located far away from the sample so as to avoid scattering of neutrons into the analyzer-detector area. There are 11 analyzer-detector arms on both sides of the neutron beam and 13 detectors clustered at low and high angles for diffraction measurements. The beryllium filters (nominal thickness 15.24 cm) are kept at $\sim 78 \text{ K}$ by an automated liquid-nitrogen cooling system. A low-efficiency BF_3 proportional gas detector is employed for monitoring the incident spectrum. Either a cylindrical ($6\text{-}12 \text{ mm}$ in diameter, up to 95 mm in height) or slab ($12\text{-}16 \text{ mm}$ in width and 95 mm in height) sample geometry can be used.

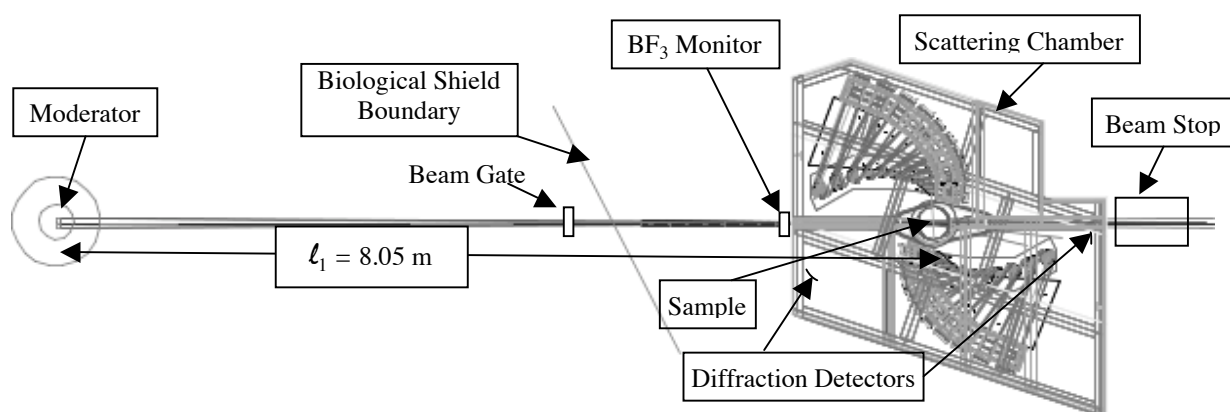


Figure 1. A schematic layout of QENS flightpath from moderator to endstation.

A more detailed top view of the crystal-analyzer and detector configuration is given in Fig. 2 and the perspective of the analyzer assembly is shown in Fig. 3. The analyzer of each arm consists of tiled pyrolytic graphite crystals (25mm x 25mm, (002) reflecting planes with a mosaic spread (FWHM) of $\sim 3.5^\circ$) on a curved surface defined by a supporting frame. In general, an equal mean distance is maintained between sample-to-analyzer (l_2) and analyzer-to-detectors (l_3) for each arm. But the dimensions of the analyzer, flight distances and number of detectors, as listed in Table 1, vary among the arms of different mean scattering angles (ϕ). Fig. 2 shows the 11 arms at $\phi \geq 90^\circ$. The corresponding arms for $\phi \leq 90^\circ$ can be generated by rotating the assembly by 180° about the vertical axis at the sample position. All the detectors are ^3He proportional counters (6.4 mm in diameter and 12.7 cm in length, 10 atm. ^3He pressure). Details of the electronics and data-acquisition systems were given elsewhere.[2]

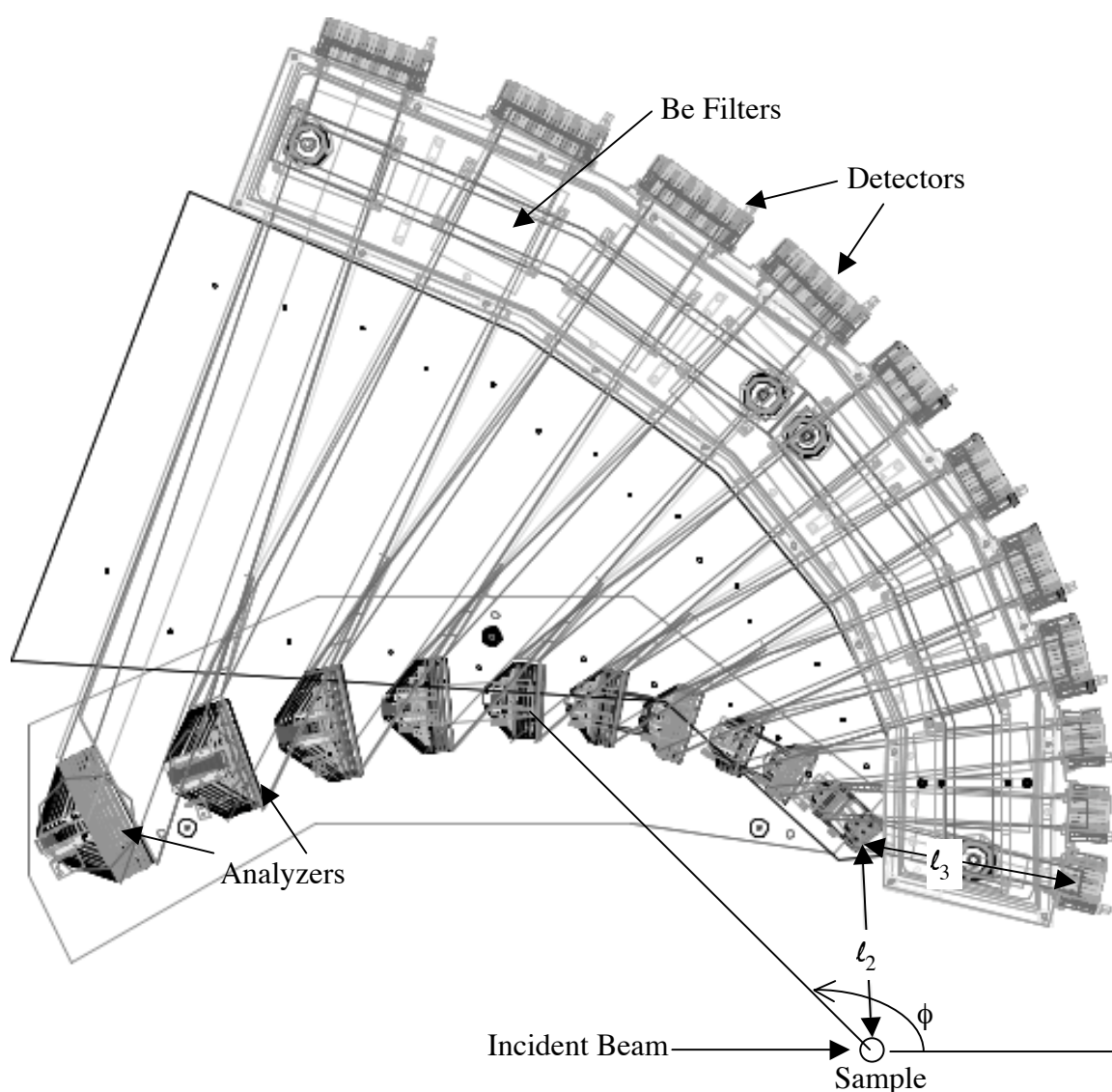


Figure 2. A top view of the analyzer, Be filter, and detector configuration for scattering angles $\phi \geq 90^\circ$. The other 11 arms, corresponding to $\phi \leq 90^\circ$, can be generated from a rotation of 180° about a vertical axis at the sample position.

Optimization of the energy resolution of the instrument depends on a number of factors: incident and scattering flight distances, dimensions and configuration of analyzer and detectors, mosaic spread of analyzer crystal planes, sample geometry, practical constraints

(e.g., space and shielding consideration), etc. Here, we only describe briefly the major design factors.



Figure 3. A photograph showing 11 analyzer crystal arrays from $\sim 90^\circ$ -scattering to near-back-scattering geometry.

First, the analyzer locus (of which defines the orientation of the crystal reflection planes) on the horizontal scattering mid-plane (where ℓ_1 , ℓ_2 , and ℓ_3 intersect the vertical centers of the sample, crystal analyzers and detectors, respectively) is considered. Apart from the uncertainties associated with ℓ_1 , t_0 (emission time from moderator), and the mosaic spread of the analyzer crystal planes, the resolution of energy transfer $E = E_i - E_f$ (where E_i and E_f are the incident and final energy, respectively), δE , depends on the variations δE_f , δt_{sd} , and $\delta \theta_B$ where t_{sd} is the sample-to-detector flight time and θ_B is the Bragg angle of the reflecting crystal planes of the analyzer. In general, δt_{sd} and $\delta \theta_B$ are coupled by the configuration of the analyzer and detector loci (neglecting the finite sample size). Application of the technique of time-focusing, which demanding a constant t_{sd} for all ℓ_2 and ℓ_3 trajectories connecting different locations on the analyzer and detector loci, is a must in order to attain good resolution. In general, time-focusing can be achieved only for scattering processes over certain region of energy transfers. One way to ensure constant t_{sd} , as used for instruments CAT [3] of KENS, TFXA [4] of ISIS and CHEX [5] of IPNS, is to arrange the analyzer and detector loci as parallel straight lines parallel perpendicular to the incident direction. Then $t_{sd} \sim (\ell_1 + \ell_2) \sin \theta_B = \text{constant}$ as θ_B changes as ℓ_1 and ℓ_2 are connected at a different point on the analyzer line. However, E_f varies and δE_f becomes a dominant contribution to the resolution for $E_f \approx E_i$, which is not desirable for a quasielastic scattering spectrometer. The QENS analyzer loci are designed to fulfill the condition of $\delta \theta_B = 0$, or equivalently *constant final-energy focusing* ($\delta E_f = 0$). [6] This can be achieved by placing the analyzer crystals on a circular locus which passes through the sample (approximated by a point) and a detector point. If we define the sample location at the origin $(0, 0)$ and the detector at $(0, \ell_{sd})$ on the x -axis and choose a Bragg angle θ_a , the circular locus is centered at $(\ell_{sd}/2, -\ell_{sd} \cot(2\theta_a)/2)$ with a radius $r = \ell_{sd} \csc(2\theta_a)/2$. For an analyzer crystal at point (x, y) on the locus, the angle between the crystal reflecting plane and the x -axis must be set equal to $\sin^{-1}((x - \ell_{sd}/2)/r)/2$. The curved analyzer loci can clearly be seen in Fig. 3. In reality, since the circular locus is approximated by joining crystal tiles that have a finite width, $\delta \theta_B$ is not truly zero.

Second, the choice of Bragg angles for each of the final-energy-focused analyzer arm is governed by the requirement of constant energy resolution for all the analyzer-detector arms. The major factor is the varying ℓ_2 (and $\ell_3 = \ell_2$), which results in a larger θ_a for a shorter arm. After the definition of the analyzer locus which is optimized for final-energy-focusing at one (point) detector, there comes the question of how to arrange detectors adjacent to this central position. All the QENS detectors (^3He cylindrical tubes) are mounted vertically and centered on the mid-plane of scattering. For each arm, there are a number of detectors aligned on both sides of the central detector along a straight line perpendicular to the central, optimized ℓ_2 . These adjacent detectors are not fully focused but, due to the mosaic distribution of the crystal reflecting planes, the focusing condition is still satisfied for a certain portion of the crystal planes, albeit with reduced intensities.

Finally, the out-of-plane configuration of the analyzer crystal array has to be considered. Thus far the optimized analyzer locus is obtained for the triangle defined by ℓ_2 , ℓ_3 , and ℓ_{sd} lying on the mid-plane of scattering. Such optimization can be maintained (for detector points on the mid-plane of scattering) if the out-of-plane analyzer surface is generated by rotating the in-plane locus about ℓ_{sd} . Accordingly, the QENS analyzer crystals are placed on such surfaces, as can be seen in Fig. 3, each spanning a vertical acceptance angle from the sample approximately -15° to $+15^\circ$. In reality, the finite detector length also contributes to the resolution effect.

Table 1: Parameters for the analyzer-detector arms of QENS

Arm [§]	$\phi(^{\circ})$	$\ell_2=\ell_3(\text{cm})$	$\theta_B(^{\circ})$	$E_f(\text{meV})$	Analyzer area (cm^2)	No. ^3He counters*
1	93.5	0.61	53.7	2.83	74	3
2	100.5	0.70	52.1	2.95	99	4
3	107.5	0.81	51.0	3.04	167	4
4	114.5	0.92	50.2	3.11	185	5
5	121.5	1.05	49.6	3.17	271	6
6	128.5	1.19	49.0	3.23	296	6
7	135.5	1.35	48.5	3.28	345	7
8	142.5	1.53	48.1	3.32	469	8
9	149.5	1.73	47.7	3.37	629	9
10	156.5	1.94	47.3	3.41	740	10
11	163.5	2.19	47.0	3.44	907	11

*Cylindrical tube: ID = 6.4mm, height = 12.7cm, ^3He pressure = 10 atm.

§Same parameters for corresponding arms at scattering angles $180^\circ - \phi$.

Recently, Carpenter and coworkers have reported a general analysis [7] and practical expressions [8] of time-focusing of pulsed-source crystal analyzer spectrometers. The QENS time-focusing with respect to constant final energy for the analyzer locus and the central detector in the scattering mid-plane is consistent with the optimal time-focusing scheme outlined by Carpenter.[7] However, the detector loci and out-of-plane analyzer-detector configuration may not be optimal. A quantitative analysis of such effects on the resolution as compared to the optimal configuration has not been done. Nevertheless, given the practical constraints of space available and mitigation of efforts in shielding and

detector installation for QENS, the present configuration is a reasonable compromise. Indeed, the observed energy resolution, as shown in Fig. 4a, agrees well with the expected specification of the instrument.

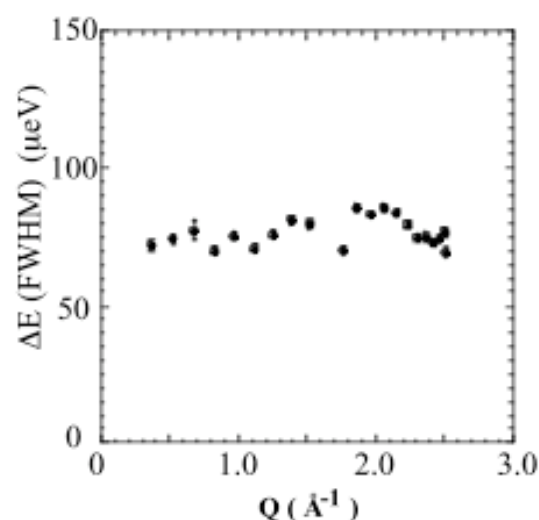


Figure 4a. The energy resolution (full-width-at-half-maximum) of QENS at the elastic position obtained from fitting the elastic-peak data of a vanadium rod by a Gaussian function. The missing data point at $Q=1.65 \text{ \AA}^{-1}$ is due to a low signal-to-noise problem in one short analyzer-detector arm.

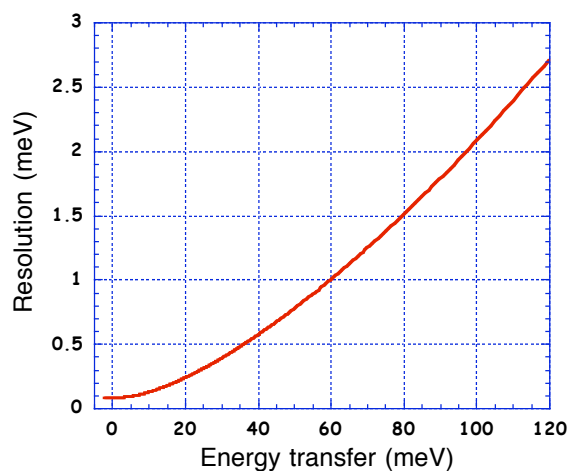


Figure 4b. The calculated energy resolution (full-width-at-half-maximum) of QENS in the elastic region.

3. Data analysis software and scientific examples

Normally, background scattering is removed from a sample run by subtracting the corresponding empty-cell run. This is important particularly when ancillary equipment for sample environment is in use, e.g., cryostats, displacer refrigerators, furnaces, and gas-handling cells, which QENS routinely provides. Measurement of incoherent scattering from a vanadium standard provides intensity normalization of the detectors and an empirical definition of the elastic energy resolution. Data analysis software based on Fortran, Genie, and IDL is available. The IDL codes are the most developed, enabling visualization of raw data, spectral normalization, conversion to $S(Q, E)$ and related scattering functions, etc. in a fairly user-friendly manner. Various ASCII files are generated for further analysis by users, especially those who may not have IDL licenses.

The first scientific example is to illustrate the capability and benefit of concurrent, parametric measurements of diffraction and quasielastic-to-inelastic scattering on QENS. In a recent study of an yttrium-doped barium cerate proton-conducting ceramic, $\text{BaY}_{0.2}\text{Ce}_{0.8}\text{O}_{3-\delta}$ (YBC), the QENS experiment enabled a simultaneous characterization of the structural response of the crystalline matrix to hydrogen incorporation and the proton dynamics in the material. Fig. 5a shows the diffraction patterns of the 10-min runs at every 10 degree as the sample was heated from 100° to 580°C in a moist atmosphere. A structural transformation of the lattice is clearly evident, as shown by the merging of two peaks around the d-spacing of 2.2 \AA into one peak at about 350°C . This structural change of the YBC crystal lattice can be correlated with the proton dynamics by analyzing the elastic scattering from hydrogen (Fig. 5b). We analyzed the integrated elastic-peak intensity according to incoherent scattering of hydrogen

as a function of Q for each temperature of the 10-min runs and obtained the mean-square displacement for the hydrogen thermal motion. The mean squared displacement as a function of temperature, as shown in Fig. 5c, indicates an abrupt change in the proton motion at 336°C which coincides the structural transformation temperature of the YBC lattice.[9] Furthermore, the quasielastic component provided a measure of the single-particle motion corresponding to the diffusion of hydrogen atoms through the YBC lattice. For example, a fit of the quasielastic component with a central peak and a single Lorentzian function implied a diffusion coefficient of $1.5 \times 10^{-5} \text{ cm}^2/\text{sec}$ at 550°C. Concurrently, QENS also measures the hydrogen vibrational modes up to about 200 meV, as shown in Fig. 5d. The ability of *in-situ* measurements of structure and dynamics at one setting is unique to QENS and valuable to many scientific investigations.

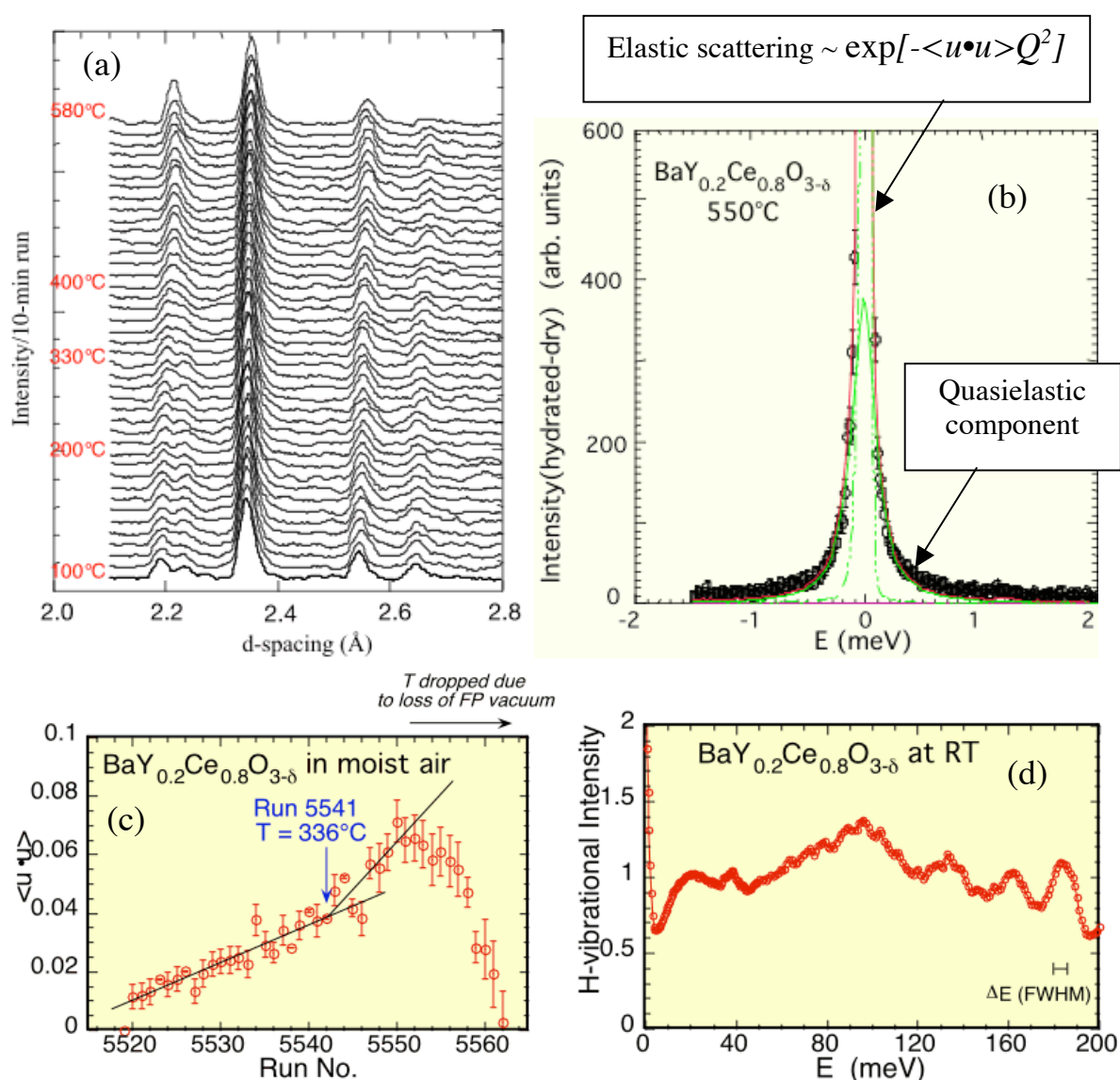


Figure 5. Concurrent diffraction and spectroscopic measurements of a proton-conducting ceramic heated-treated in a moist N_2 atmosphere.

Another example is to investigate the effects of nanoscale confinement on the structure and dynamics of polyethylene oxide (PEO) in a silica based hydrophilic porous glass, Vycor. The crystalline nature, as revealed by the Bragg peaks around 1.5 Å from an h-PEO film, is

strongly suppressed when PEO is confined in Vycor (see Fig. 6a). Consequently, the relaxation processes of the confined sample are expected to be different from those of the bulk. It was shown previously [10] that the local relaxation in bulk PEO obeys a Kohlraush-Williams-Watts (KWW) function as $\exp[-(t/\tau)^\beta]$, where τ is a relaxation time and $\beta < 1$ is the 'stretch exponent' that controls the extension of the decay process in time (t). In order to differentiate this behavior from the others, high quality quasielastic-scattering data are required. First, the mean-square displacement associated with hydrogen vibrations shows distinct temperature dependence at the melting point between the free and confined PEO, see Fig. 6b. The slowing-down effect due to confinement is manifested by the reduced mean-square displacement in the confined sample at ~ 373 K. Furthermore, an analysis of the QENS data successfully identified the presence of a broad Lorentzian component in addition to the KWW function for PEO in Vycor and permitted a quantitative determination of all the parameters: the Lorentzian relaxation time τ_0 , as well as the KKW τ and β as a function of Q . The results are shown in Fig. 6c and 6d. Experimental details and an alternative use of the KWW function for data treatment of polymer melts are given elsewhere. [11]

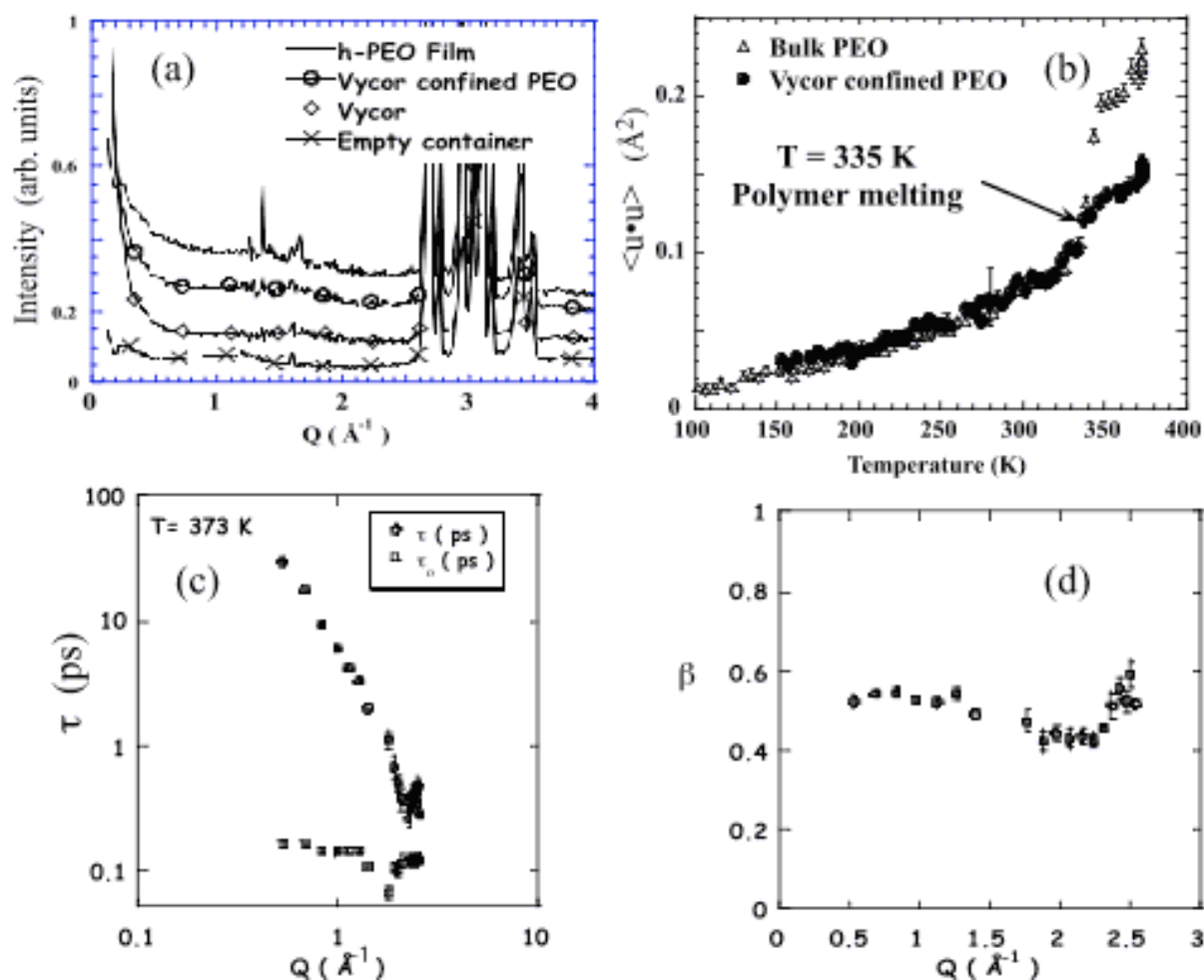


Figure 6. (a) Diffraction data from different unconfined and confined PEO and Vycor and empty references. In addition to the suppression of the PEO Bragg peaks in the confined sample, strong small-angle scattering from the microstructure was observed. (b) The temperature dependence of the mean-square displacement. (c and d) The parameters of relaxation functions obtained from the QENS data (see text).

4. Future improvements

A significant improvement of the QENS hardware can be realized by installing a funnel guide system upstream of the sample position. The present QENS configuration permits a $\sim 7^\circ$ horizontal acceptance angle of the scattered beam at the analyzer crystals but only intakes a minute ($< 1^\circ$) view of the incident beam at the sample. Therefore, recovering the escaped phase space of the incident beam, to be achieved by a funnel guide, will significantly increase the flux (especially for long-wavelength neutrons) at sample without sacrificing the (Q , E) resolution. A design study of a funnel guide (using $m = 3.6$ supermirror coating on borofloat glasses) consisted of six tapered, rectangular cross-section segments approximating an elliptically focusing was completed. The calculated gain factors of neutron fluxes at different wavelengths are given below:

Wavelength (Å)	Gain factor (no funnel=1) Elliptically focused guide
8	3.5
4	2.3
2	1.55
1	1.0

The guide system is currently being manufactured by SwissNeutronics and will be delivered and installed on QENS in the summer of 2003. The large gain of incident intensities provided by the funnel guide will have a significant impact on improving the turn-over time of data collection and data quality.

Another project is to rectify the high background currently observed in the short-arm detectors near $\phi = 90^\circ$. This problem is probably due to the lack of space for shielding materials in this area (see Fig. 2). We shall improve the signal-to-noise ratio in these detector arms by employing more effective shielding.

We shall continue to improve the user-friendliness of the IDL data-analysis codes. Eventually, we hope that the data treatment software for QENS will expand to network-based, platform-independent, I/O-standardized, and free-of-charge systems, such as the Integrated Spectral Analysis Workbench (ISAW) that has been developed for neutron data visualization and analysis and IPNS.[12] As far as the data acquisition system is concerned, QENS is in line for the upgrade to the next-generation hardware and software. This new system has been successfully installed on HRMECS and SCD and has brought new capabilities and better reliability to the operation.

Acknowledgement

Work performed at Argonne National Laboratory is supported by the U. S. DOE-BES under the Contract No. W-31-109-ENG-38.

References

- [1] K. F. Bradley, S.-H. Chen, T. O. Brun, R. Kleb, W. A. Loomis, and J. M. Newsam, *Nucl. Instr. Methods*, **A270**, 78 (1988).
- [2] R. K. Crawford, R. T. Daly, J. R. Haumann, R. L. Hitterman, C. B. Morgan, G. E. Ostrowski, and T. G. Worlton, *IEEE Trans. Nucl. Sci.* **NS-28**, 3692 (1981).
- [3] N. Watanabe, S. Ikeda, and K. Kai, in ICANS VI Proceedings, Argonne National Laboratory, Report ANL-82-80, p.280

In "*The 16th Meeting of the International Collaboration on Advanced Neutron Sources*", edited by G. Mank and H. Conrad (Forschungszentrum Jülich GmbH, Jülich, Germany, Düsseldorf-Neuss, Germany, 2003), Vol. I, p. 279-288.

- [4] J. Penfold, J. Tomkinson, "The ISIS Time Focused Crystal Spectrometer, TFXA", Rutherford-Appleton Laboratory Report RAL-86-019 (1986).
- [5] C. N. Tam, P. Bour, J. Eckert, F. R. Trouw, *J. Phys. Chem.* **A101**, 5877 (1997).
- [6] R. K. Crawford, F. Trouw, and H. A. Belch, IPNS Notes No. 79 (1997), unpublished.
- [7] J. M. Carpenter, *Nucl. Instr. Methods*, **A483**, 774 (2002).
- [8] J. M. Carpenter, E. B. Iverson, and D. F. R. Mildner, *Nucl. Instr. Methods*, **A483**, 784 (2002).
- [9] K. Takeuchi, C.-K. Loong, J. W. Richardson, Jr., J. Guan, S. E. Dorris, and U. Balachandran, *Solid State Ionics* **138**, 63 (2000).
- [10] G. Mao, R. Fernandez Perea, W. S. Howells, D.L. Price, and M.-L. Saboungi, *Nature* **405**, 163 (2000).
- [11] J.-M. Zanotti, L.J. Smith, E. Giannelis, P. Levitz, D.L. Price and M.-L. Saboungi, Proc. *MRS Symposium*, Boston, MA, November 2002, in press; J.-M. Zanotti, L.J. Smith, D.L. Price and M.-L. Saboungi, PRL, submitted.
- [12] T. G. Worlton, P. F. Peterson, A. Chatterjee, J. P. Hammonds, D. J. Mikkelsen, and R. L. Mikkelsen, (unpublished); <http://www.pns.anl.gov/computing/isaw/>.